316 *Macromolecules* **2010**, *43*, 316–325
DOI: 10.1021/ma902303e

Macromolecules
ARTICLE

# $CO_2$ Transport in Polysulfone Membranes Containing Zeolitic Imidazolate Frameworks As Determined by Permeation and PFG NMR Techniques

**Kenya Díaz,[†] Leoncio Garrido,[‡] Mar López-González,[‡] Luis F. del Castillo,*[,†] and Evaristo Riande*[,‡]**

[†]*Departamento de Polímeros, Instituto de Investigaciones en Materiales, Universidad Nacional Autónoma de México, Ap. Postal 70360, Coyoacán, México DF, México, and* [‡]*Departamento de Química Física, Instituto de Ciencia y Tecnología de Polímeros (CSIC), 28006 Madrid, Spain*

*Received August 6, 2009; Revised Manuscript Received November 10, 2009*

ABSTRACT: This work describes the preparation of mixed matrix membranes by casting from poly(1,4-phenylene ether−ether−sulfone) chloroform solutions containing dispersed zeolitic imidazolate frameworks. Diffusive studies of $CO_2$ in the pristine poly(1,4-phenylene ether−ether−sulfone) membrane and composite membranes were performed at 6 bar and 298 K, using pulsed field gradient NMR techniques. The evolution of the heterogeneity of the diffusion environments as seen by NMR was monitored in terms of the diffusion time and a stretching parameter. The values of the self-diffusion coefficient increase with filler content, from $2.1 \times 10^{-8}$ cm$^2$ s$^{-1}$ for pristine membranes to $9.3 \times 10^{-8}$ cm$^2$ s$^{-1}$ for membranes with 30 wt % of filler. Sorption and permeation experiments carried out at different pressures were used to determine the dual-mode model parameters that describe the transport processes. Apparent diffusion coefficients of $CO_2$ in the membranes were obtained from the time lag method, from parameters of the dual-mode model, and directly from the derivatives of the steady flux, expressed in terms of concentration and pressure, with respect to pressure. In general, the values of the apparent diffusion coefficients obtained by the three methods for pristine membranes are in rather good agreement with the self-diffusion coefficient obtained by the NMR technique. In composite membranes, the values of the self-diffusion coefficients are nearly 2 times those obtained using permeation and sorption experiments. The discrepancies between the values of the self-diffusion coefficients and the results obtained for the diffusion coefficient by other techniques are discussed. The filler contributes greatly to gas permeation by increasing the gas solubility in the composite membranes.

## Introduction

To surpass the trade-off between selectivity and permeability marked by the upper bound curves developed by Robeson[1] for gas separation in polymeric membranes seems to be a task difficult to achieve.[2] In principle, the addition of inorganic materials such as carbon molecular sieves or zeolites into a polymer matrix could enhance the membrane performance above the Robeson's limit.[3,4] However, mixed matrix membranes (MMMs) present some limitations, in many cases arisen from poor interactions between inorganic fillers and glassy polymers that can lead to the formation of nonselective voids, resulting in Knudsen flow.[5] This problem can be alleviated by modification of the external surfaces of zeolites with silane coupling agents, but this process presents the drawback that they can block pore access.[6] MMMs can also be prepared functionalizing the surface of mesoporous silica with reactive silanol groups in order to favor filler−matrix interactions.[7] Other fillers such as inorganic oxides,[8−10] fullerenes,[11] and nanotubes[12] also need to be functionalized to improve filler−matrix adhesion.

Metal−organic frameworks (MOF) have emerged as a new family of nanoporous materials. Known as coordination polymers, MOFs are crystalline materials made up of metal ions (or clusters) and organic ligands.[13,14] The flexibility to design functionalized structures compatible with polymers renders MOFs especially attractive for gas storage and to prepare MMMs for gas separation.[15] Though most studies related with MOFs are focused on their use for adsorption of methane[16−18] and hydrogen,[19−21] some of these materials have also shown high capacity for $CO_2$ storage.[22] Since gases involved in industrially important separations including $H_2$, $CH_4$, $CO_2$, $O_2$, and $N_2$ are selectively adsorbed in MOFs, the incorporation of these porous materials in glassy membranes may enhance gas permeability without losing selectivity.[23]

Imidazolate frameworks (ZIFs) are a new class of MOFs with tetrahedral networks that resemble structure type zeolites. The tetrahedral Si(Al) and the bridging oxygen in zeolites are replaced respectively by transition metal ions (Zn, Co) and imidazolate link, in ZIFs. Notice that the angle M−IM−M, where M and IM represent respectively the coordination metal and the imidazolate group, is similar to that of O−Si−O in zeolites (145°).[24] Whereas the structure of silicate-based zeolites is templated by structure-directing agents (SDAs), typically amines that remain as extra-framework entities, the structure adopted by ZIFs depends on both the type of substitution (methyl, benzyl, etc.) in the imadazolate group and the solvent used. Then, the great structural variety of ZIFs begins with the functionalization of the imidazolate linkers. ZIFs capture $CO_2$ from different gas mixtures, and this characteristic combined with thermal and chemical stability and high surface area makes these materials promising candidates for $CO_2$ storage.[25,26]

In view of the antecedents, the study of the effect of ZIFs on the transport of $CO_2$ in MMMs membranes was undertaken in this work. Poly(1,4-phenylene ether−ether−sulfone) (PPEES), a high thermal stability polymer with good mechanical properties, and ZIF-8 were chosen as components of MMMs. ZIF-8, which

*Correspondence authors. E-mail: lfelipe@servidor.unam.mx (L.F.d.C.); riande@ictp.csic.es (E.R.).

 Published on Web 11/20/2009 

consists of $ZnN_4$ clusters linked by 2-methylimidazole, has an excellent thermal stability. The presence of ZIF-8 in the MMMs may increase the variety of paths through which gases diffuse. Traditionally, the diffusion coefficient of gases is obtained from permeation curves so that a concentration gradient is involved in the measurements. More reliable information on gas diffusivity in membranes may presumably be obtained from the self-diffusion coefficient of gases determined from the trajectories of the diffusant particles in the membranes. The measurements of self-diffusion coefficients involve the use of microscopic experiments such as the pulsed field gradient (PFG) NMR spectroscopy. This technique has been widely utilized to measure self-diffusion coefficients of fluids in bulk and confined geometries,[27,28] but its use to investigate gas diffusive processes in dense membranes is relatively scarce. To our knowledge, no PGF NMR studies on gas diffusivity in composite membranes have been reported. This nondestructive method of measuring molecular mobility at the mesoscopic level is attractive because permits to determine self-diffusion coefficients from averaging the square root of the mean-square end-to-end distance of the diffusion trajectories. Then, one of the main goals of this work is to compare the self-diffusion coefficient of $CO_2$ estimated by PGF NMR with the apparent diffusion coefficients obtained with methods used commonly that are based on macroscopic procedures.

Although this work is mainly focused on the effect of ZIFs upon gas diffusion, the influence of ZIF-8 on the solubility of $CO_2$ in the composite membranes was also investigated. Sorption and desorption measurements were performed at several pressures in MMMs containing different fractions of ZIF-8. The results obtained in combination with the permeation results were used to estimate the effect of ZIF-8 on the parameters of the dual-mode model proposed to describe the transport of $CO_2$ in the glassy membranes.[29,30] Special attention was also paid to the effect of ZIF-8 density on the permeation properties of the MMMs. In this regard, it should be pointed out that the skeleton density of the ZIF-8 is nearly 4 times that of the original MOF, and the pore aperture is 3.4 Å, allowing it to readily absorb small molecules such as $CO_2$.[24] Possible migration of the polymer chains into the pores of the filler is discussed.

## Experimental Part

**Materials.** The zeolitic imidazolate framework containing $Zn^{2+}$ as coordinate metal (ZIF-8) was supplied by Aldrich. Values of the particles density, particle size, and BET surface area, all of them supplied by Aldrich, were respectively 0.35 g cm$^{-3}$, 4.9 $\mu$m, and 1300−1800 m$^2$ g$^{-1}$. Poly(1,4-phenylene ether−ether−sulfone) (PPEES) was also supplied by Aldrich, with an approximate molecular weight of 26 000 g mol$^{-1}$ and $T_g$ about 463 K.

**Powder X-ray Diffraction.** X-ray powder diffraction data were collected on a Bruker D8 Advance powder diffractometer using Cu K$\alpha$ radiation, $\lambda$ = 1.5418 Å. The pattern was scanned over an angular range of 5°−60° (2$\theta$) with a step size of 0.0167° s$^{-1}$. The phase of the ZIF-8 was confirmed by a comparison of simulated from single-crystal X-ray data.[24] The diffractogram of the ZIF-8 sample was directly indexed utilizing the program Dicvol,[31] using the 10 most intense peaks. A cubic unit cell was found with cell parameters $a$ = 16.99(3) Å, $\alpha = \beta = \gamma$ = 90°, and $V$ = 4906.7(1) Å$^3$, where the numbers in the parentheses are standard deviations in the last significant digits. The calculated cell parameters are consistent with those reported for ZIF-8.[24] The crystal structure of ZIF-8 is shown in Figure 1, and the density of the cell unit is 0.93 g cm$^{-3}$.

**Membranes Preparation.** Pristine poly(1,4-phenylene ether−ether−sulfone) (PPEES) membranes were cast from chloroform polymer solutions at room temperature. The mixed matrix membranes were prepared by mixing ZIF-8 and PPEES. Briefly, ZIF-8 fine powder was slurred into chloroform and sonicated to disperse the powder. The ZIF-8 dispersion was added under strong stirring to a chloroform polymer solution containing the amount of polymer necessary to prepare the desired MMM. The mixture was sonicated for several time periods until an apparently homogeneous suspension was observed. As an example, the preparation of a membrane containing 0.10 mass fraction of ZIF-8 was carried out by slurring 40 mg of fine powder of this material in 5 mL of chloroform, which was further added to a dilute chloroform solution containing 360 mg of PPEES under strong stirring. Then, the mixture was sonicated at room temperature for 1 h, vigorously stirred for another hour, and finally sonicated for an additional 30 min. Membranes were cast onto a Teflon mold. After casting and to avoid bubble formation, the MMM of interest was dried in vacuum at 333 K overnight. Then, the temperature of the membrane was increased up to 473 K at intervals of 20 K, and the system was kept in each step for 4 h. After reaching 473 K, the membrane was cooled to room temperature, and the system was kept at this temperature under vacuum. In what follows, the acronyms used for the MMMs will be MMM-*XX*, where *XX* is the percentage of ZIF-8 in the composite.

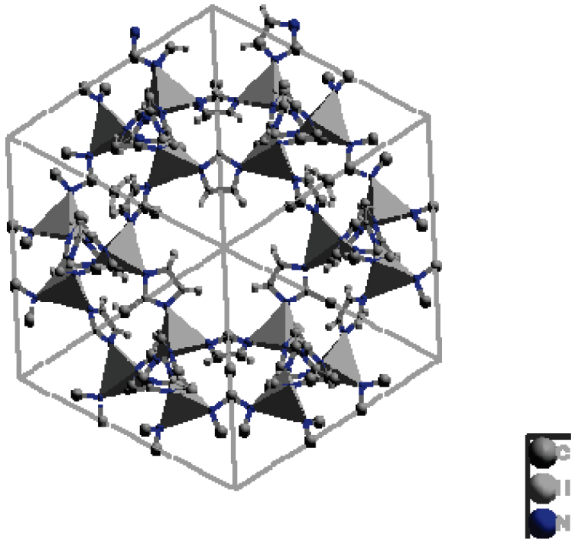

**Figure 1.** A 3D open framework view of the crystalline structure of ZIF-8, calculated using Diamond 3.1 software and the Crystallographic Information File (CIF) of ref 24. The tetrahedral consists of $ZnN_4$ clusters connected by 2-methylimidazolate linkers. For clarity, some H atoms on the linkers are not shown.

**Density.** Solvent occluded in the fillers of MMMs as a result of the cast process was totally removed at 473 K under high vacuum. Then, the bulk density of the MMMs was measured by pycnometry, at 303 K, using isooctane, and the results obtained are given in the third column of Table 1. It is worth noting that the high molecular volume of isooctane precludes its diffusion across the polymer-ZIF-8 interface into the pores of the filler.

**Scanning Electron Microscopy.** The films were fractured under liquid nitrogen. Cross-sectional surfaces of the membranes were sputter-coated with gold−palladium before examination under a Philips XL 30 SEM apparatus with tungsten filament.

**Thermal Analysis.** Differential scanning calorimetry (DSC) experiments were performed at 10 K min$^{-1}$ using a Pyris 1 apparatus (Perkin-Elmer) under a nitrogen atmosphere. Thermogravimetric analysis (TGA) of the membranes was carried out using a TA Q-500 device at a heating rate of 10 K min$^{-1}$ under a nitrogen atmosphere.

**Table 1. Values of the Dual-Mode Model Parameters for the Sorption and Desorption of Carbon Dioxide for Polysulfone (PPEES) and MMMs Membranes at 303 K**

| process | sample | density, g cm$^{-3}$ | $k_D \times 10^2$, cm$^3$ (cm$^3$ cmHg)$^{-1}$ | $b \times 10^3$, (cmHg)$^{-1}$ | $C'_H$, cm$^3$ cm$^{-3}$ |
|---|---|---|---|---|---|
| | ZIF-8 | 0.35[a] | | | |
| sorption | PPEES | 1.24 | 1.72 | 11.2 | 8.1 |
| | MMM-10 | 1.21 | 2.91 | 5.8 | 9.6 |
| | MMM-20 | 1.14 | 3.67 | 5.1 | 12.9 |
| | MMM-30 | 1.15 | 2.75 | 1.8 | 40.9 |
| desorption | PPEES | | 1.15 | 54.1 | 18.3 |
| | MMM-30 | | 1.65 | 2.1 | 62.8 |

[a] Value supplied by Aldrich.

**PFG NMR Experiments.** Membrane strips less than 800 $\mu$m wide and ~2 cm long were placed inside a thick-wall 10 mm o.d. NMR tube designed for NMR studies of pressurized gases. Prior to fill the tube at a given pressure with [$^{13}$C]$O_2$, the air was removed by vacuum. Unless indicated otherwise, the gas pressure used in these experiments was about 6 bar to facilitate the measurements with adequate signal-to-noise ratio in a reasonable amount of time. The gas pressure was monitored with a transducer working in the range 0−10 bar. The self-diffusion coefficient of the gas in the membranes was estimated by a spin-echo type of radio-frequency (rf) pulse sequence, as shown by Stejskal et al.[32] Briefly, the measurements were performed in a Bruker Avance 400 spectrometer equipped with a 89 mm wide bore, 9.4 T superconducting magnet ($^{13}$C Larmor frequency at 100.61 MHz). The reported data were acquired at 298 ± 1 K with a Bruker diffusion probehead Diff60 using 90° $^{13}$C rf pulse lengths of about 13 $\mu$s. The diffusion time, $\Delta$, was varied between 10 and 1500 ms, using a pulsed field gradient stimulated spin-echo sequence. The length of the field gradient pulses, $\delta$, varied between 1 and 2 ms. For each pair of $\delta$ and $\Delta$ values, the amplitude of the gradient pulses varied from 0 up to a maximum value of 18 T m$^{-1}$. The repetition rate was 15 s. The total acquisition time for these experiments ranged from 3 to 25 h. The self-diffusion coefficient at a given $\Delta$ was calculated by fitting the experimental data to the corresponding exponential function. Previous to the measurements, the field gradient was calibrated following the spectrometer manufacturer's protocol at 298 ± 1 K, using a sample of water doped with $CuSO_4$ at 1.0 g L$^{-1}$ and a value of the water diffusion coefficient equal to $2.3 \times 10^{-5}$ cm$^2$ s$^{-1}$. Furthermore, the calibration was verified at the range of gradient values used experimentally by measuring the diffusion coefficient of dry glycerol. It was found a value of $D = 2.23 \times 10^{-8}$ cm$^2$ s$^{-1}$, in good agreement with the results reported for this parameter elsewhere.[33] Also, diffusion measurements for these two liquids were performed over a wide range of diffusion times to assess the stability of the gradients and whether artifacts due to eddy currents could affect the measurements.

**Permeation Experiments.** Permeation measurements were performed in an experimental device consisting of a stainless steel permeation cell which separates an upstream pressure chamber from a downstream pressure chamber by means of a membrane that exposes an area of 3.464 cm$^2$ to the gas. The permeation device was immersed in a water thermostat. After making vacuum in the two compartments of the permeation cell, carbon dioxide at a predetermined pressure was allowed to flow into the upstream chamber. The pressure of the gas in the latter chamber was measured with a Gometric pressure transducer. Gas flowing across the membrane from the upstream to the downstream chamber was monitored with a MKS 628/B transducer ($10^{-4}$−1 mmHg) via a PC. The permeation experiments were carried out at 303 K. Prior to each experiment, the air inlet was measured as a function of time and further subtracted from the pressure vs time curve recorded in the downstream chamber. The resulting $p(t)$ vs $t$ curves present a transient process at short times followed by a straight line that define steady-state flow conditions. The permeability coefficient was obtained from the slope of the straight line by means of the following expression

$$P = 3.59 \frac{Vl}{p_0 AT} \lim_{t \to \infty} \left\{ \frac{dp(t)}{dt} \right\} \quad (1)$$

where $V$ is the volume of the downstream chamber, $A$ is the permeation area, $l$ is the thickness of the membrane, and $p_0$ is the pressure of the gas in the upstream chamber. If $V$, $l$, and $A$ are given in cgs units and pressure in cmHg, the permeation coefficient is obtained in barrers, 1 barrer = $10^{-10}$ [cm$^3$ (STP) cm cm$^{-2}$ s$^{-1}$ (cmHg)$^{-1}$]. The diffusion coefficient, $D$, was determined by the method suggested by Barrer[34]

$$D = l^2/6\theta \quad (2)$$

where the time lag $\theta$ is the time at which the straight line defined by the plot $p$ vs $t$ in steady-state conditions intersects the abscissa axis. Usually $D$ is given in cm$^2$ s$^{-1}$. The apparent solubility coefficient of the gas in the membranes was obtained from

$$S = P/D \quad (3)$$

If $P$ is given in barrers and $D$ in cm$^2$ s$^{-1}$, the units of $S$ are cm$^3$ (STP) cm$^{-3}$ (cmHg) $^{-1}$. Notice that $S$ only coincides with the true solubility coefficient in the case that gas sorption in the membrane obeys Henry's law.

**Sorption Experiments.** Sorption measurements were performed at 303 K using an experimental device made up of two chambers separated by a valve.[35] The sorption device was immersed in a thermostat bath set at the temperature of interest. Circular films 0.1 mm thick, separated by metallic grids to facilitate gas sorption, were introduced into one of the chambers, called sorption chamber. After evacuated the two chambers by vacuum, they were isolated from each other by closing the valve separating them. Prior to the experiment, the evolution of the pressure in the sorption chamber was monitored as a function of time to verify that neither air nor traces of solvent were present in the samples. Then, carbon dioxide at a given pressure was introduced into the chamber that acts as reservoir, and once thermal equilibrium was achieved, the gas was allowed to flow to the sorption chamber by suddenly opening and closing the valve separating them. The evolution of pressure with time in the gas sorption chamber was monitored with a Ruska model 7230 (0−35 bar) pressure sensor via a PC.

The concentration of gas in the membranes was determined by means of the following expression

$$c = \frac{22414 \rho V}{RTm} \left( \frac{p_1}{z_1} - \frac{p_2}{z_2} \right) \quad (4)$$

where $m$ and $\rho$ are respectively the mass (g) and density (g cm$^{-3}$) of the membrane in the sorption chamber of unoccupied volume $V$ (volume of the sorption chamber minus the sum of the volumes occupied by the polymer and the metallic grids, in cm$^3$), $p_1$ and $p_2$ are respectively the starting ($t = 0$) and equilibrium ($t \to \infty$) pressures and $z_1$ and $z_2$ are the compressibility factors of $CO_2$ at the respective pressures. The concentration obtained from eq 4 is given in cm$^3$ (STP) cm$^{-3}$.

Immediately after obtaining the sorption curves, desorption experiments were carried out at 303 K using the following protocol. Let us consider that the concentration and pressure of gas in the membrane in the final sorption step are $c_f$ and $p_f$, respectively, To proceed with the desorption experiment, the valve separating the sorption cell from the evacuated reservoir was suddenly opened and closed, the pressure of gas in the sorption cell decreasing from $p_f$ to $p_{f-1}$. By effect of the desorption process taking place in the membrane, the pressure of the sorption cell increases reaching an equilibrium

pressure $p_{f-1} > p_{f-1;i}$ after a certain time $t$. The concentration of gas in the membrane in the first desorption step was calculated by means of the following expression

$$c_{f-1} = c_f - \frac{22414\rho V}{RTm}\left(\frac{p_{f-1}}{z_{f-1}} - \frac{p_{f-1;i}}{z_{f-1;i}}\right) \quad (5)$$

The same procedure was used for the subsequent steps.

## Results

DSC curves for both the pristine polysulfone membrane and the MMMs were obtained using the drying protocol described in the Supporting Information. The glass transition temperature of the membranes was found to be independent of filler content, its value lying in the vicinity of 459 K. TGA curves for the membranes do not show any loss of mass until 623 K (see Supporting Information). DSC and TGA results suggest that polymer−filler interaction does not affect the thermal behavior of the MMMs.

X-ray diffractograms presented for the PPEES, ZIF-8, and MMMs in Figure 2 indicate that the polymeric matrix does not alter the crystalline pattern of ZIF-8. Moreover, the diffractogram of PPEES reveals the amorphous nature of this polysulfone.

SEM images of activated ZIF-8 powder, shown in Figure 3a, exhibit a narrow distribution of particles with sizes lying in the vicinity of 5 $\mu$m. The zoom presented in Figure 3b shows each of these particles as an aggregate of smaller particles with sizes lying in the range of 400−500 nm. An inspection of different cross-sectional images of the MMMs, represented in Figure 4, indicates a rather homogeneous distribution of the microporous ZIF-8 in the polysulfone matrix. The size of the particles in the MMMs is less than 1 $\mu$m, suggesting that the sonication process carried out in the preparation of the membrane destroys the aggregates of the original ZIF-8 powder. The apparent absence of voids in the membranes indicates good wetting properties of the filler with the polymer matrix. MMM-10 and MMM-20 exhibit a rather good dispersion of the ZIF-8 particles in the polymer matrix. However, aggregation of particles might occur for the MMM-30, though the distribution of the filler through the membrane thickness seems to be rather homogeneous.

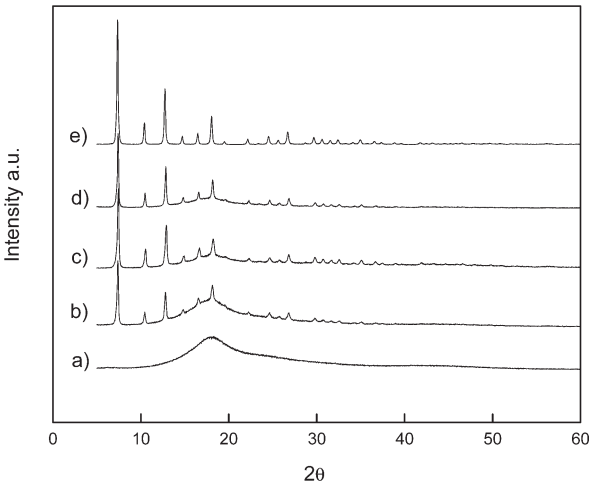


**Figure 2.** X-ray diffractogram patterns for PPEES (a), MMM-10 (b), MMM-20 (c), MMM-30 (d), and ZIF-8 (e).

The $^{13}$C NMR spectra of the membranes with carbon dioxide show two peaks associated with the $^{13}$C signal of $[^{13}C]O_2$, centered at 124.2 and 120.7 ppm (see Supporting Information). The two peaks reflect the existence of two populations of $[^{13}C]O_2$ corresponding respectively to the nonsorbed (free) and sorbed (in the membrane) gas fractions, in a slow exchange regime. The peak at lower frequency arises from interaction between the polymer/filler and gas molecules which have a highly polarizable C═O bond. A PFG stimulated spin-echo sequence was used to determine the diffusion coefficient of $CO_2$ in the membranes. The application of three $\pi/2$ rf pulses timely spaced generates an observable NMR signal (echo) centered at a time equal to $2\tau_1 + \tau_2$ (stimulated spin echo) from the first rf pulse, where $\tau_1$ is the time separation between the first two rf pulses and $\tau_2$ is the time elapsed between the second and the third rf pulses. The magnetic labeling is accomplished by applying two field gradient pulses of amplitude and duration $g$ and $\delta$, respectively, spaced by a time $\Delta$, the diffusion time. In the absence of motion, the loss of phase coherence of the NMR signal caused by the first gradient pulse would be compensated by the second gradient pulse, but this would not be the case if molecular diffusion occurs during the time $\Delta$. For illustrative purposes, $^{13}$C PFG NMR spectra corresponding to $[^{13}C]O_2$ sorbed in MMM-20 are shown as a function the amplitude of the field gradient in Figure 5. The echo attenuation can be written as[32]

$$A(g) = A(0)\exp[-(b'D)] \quad (6)$$

where $A(g)$ and $A(0)$ are the amplitude of the echo in the presence of a gradient pulse with amplitude $g$ and 0, respectively, $b' = (\gamma g\delta)^2(\Delta - \delta/3)$ where $\gamma$ is the gyromagnetic ratio of the nucleus being observed, $\Delta$ and $D$ are respectively the diffusion time and the self-diffusion coefficient of the sorbed gas, and $\delta$ is the duration of the gradient pulse. Figure 6 illustrates the attenuation of the echo intensity with increasing values of $b'$, keeping $\Delta$ and $\delta$ constant. In many cases, the experimental curves are not described by a single-exponential, but by a multiexponential fit associated with different diffusion coefficients. Since a continuum spectrum of diffusion coefficients might be a more realistic description of the systems under consideration[36] than that

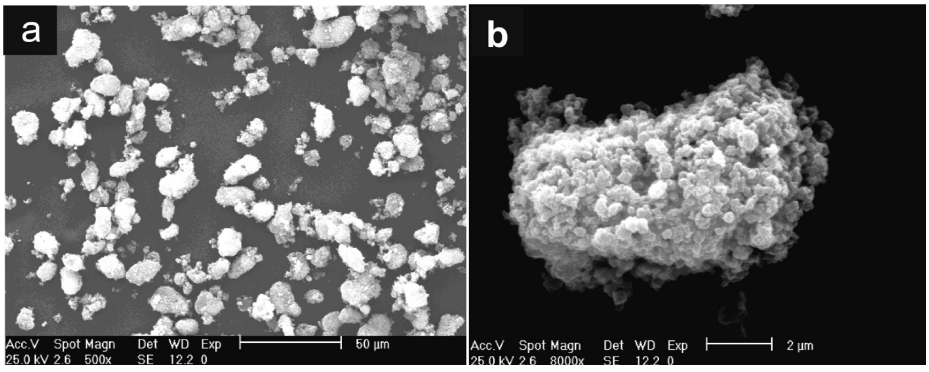


**Figure 3.** SEM micrographs for ZIF-8 particles (a) and a single particle (b).

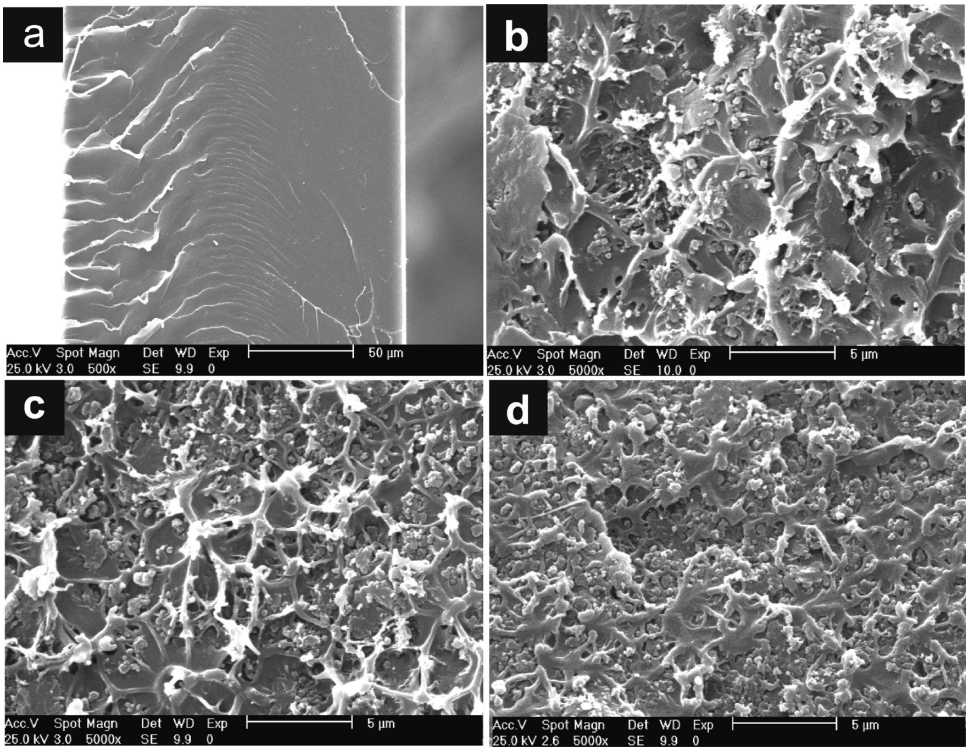


**Figure 4.** SEM micrographs showing transversal sections of (a) PPEES membrane, (b) MMM-10, (c) MMM-20, and (d) MMM-30.

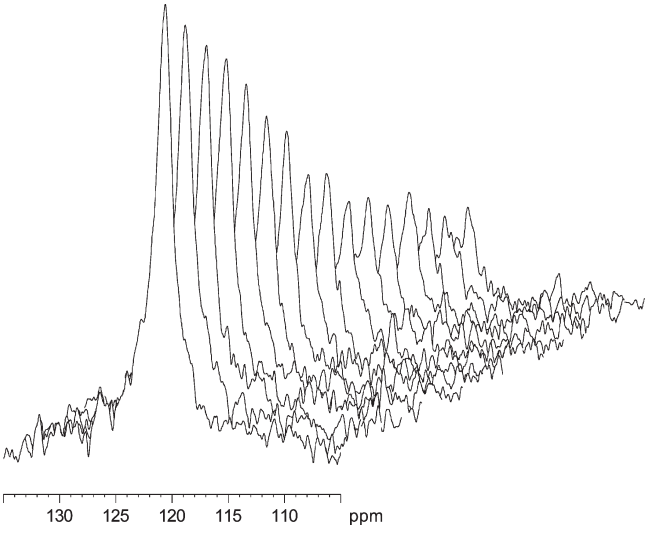


**Figure 5.** $^{13}$C PFG NMR spectra corresponding to [$^{13}$C]$O_2$ sorbed in MMM-20 obtained with a diffusion time, $\Delta$, equal to 60 ms. The duration, $\delta$, of the gradient pulse was kept constant to 2 ms, and the amplitude of the field gradient, $g$, was incremented in 16 consecutive steps of 60 g cm$^{-1}$ from an initial value of 60 g cm$^{-1}$.

provided by a set of discrete values (i.e., multiexponential fit), the data were fitted to a stretched exponential

$$A(g) = A(0)\exp[-(b'D_{app})^{\beta}] \quad (7)$$

where $\beta$ is a "stretching" parameter, $D_{app}$ is the apparent self-diffusion coefficient, and the rest of the variables are previously described. Values of $D_{app}$ obtained by means of eq 7 for a pulse gradient length of 2 ms are shown as a function of $\Delta$ for MMMs in Figure 7. In all cases, the values of $D_{app}$ decrease as $\Delta$ increases, reaching asymptotic values for $\Delta > 800$ ms. On the other hand, the values of $\beta$ increase as $\Delta$ increases, reaching values close to the

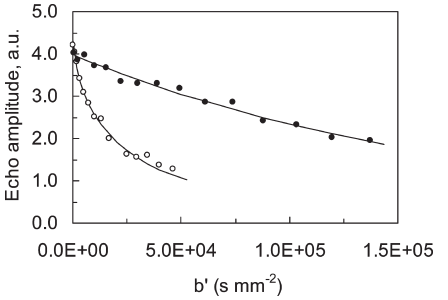


**Figure 6.** Plot of the peak intensity vs $b'$ (s mm$^{-2}$) corresponding to [$^{13}$C]$O_2$ sorbed in polysulfone with 10% (w/w) ZIF-8 obtained with a diffusion time, $\Delta$, equal to (○) 10 ms and (●) 1500 ms. The duration, $\delta$, of the gradient pulse was kept constant to 2 ms, and the amplitude of the field gradient, $g$, in G/cm, was varied between 15 and 1760. For each data point, 48 scans were averaged with a TR of 15 s. The solid lines represent the best fits to the corresponding stretched exponential (eq 7).

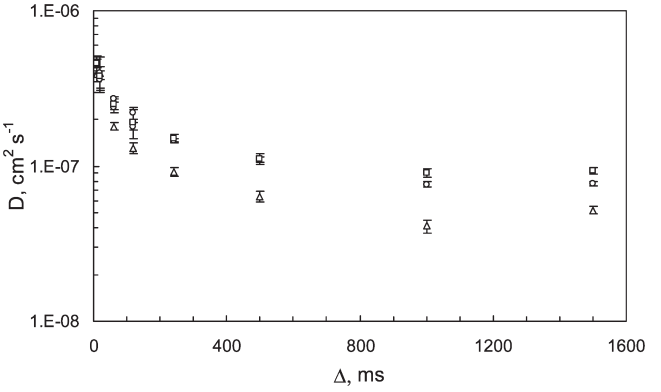


**Figure 7.** Variation of the apparent diffusion coefficient of [$^{13}$C]$O_2$ in the MMMs containing 10% (triangles), 20% (circles) and 30% (squares) w/w of ZIF-8, with the diffusion time $\Delta$. In all cases, the duration of the gradient pulse, $\delta$, was 2 ms.

**Table 2. Values of the Diffusion Coefficients of $[^{13}C]O_2$, Measured by the PFG NMR Technique, for Polysulfone Membranes, Filler, and MMMs[a]**

| ZIF-8 w/w (%) | $D_{app} \times 10^8$ ($cm^2\ s^{-1}$)[c] | $\beta$[c] | $\Delta$ (ms) |
|---|---|---|---|
| 0 | 2.1 (0.9); | 0.7 (0.2); | 20 |
| 10 | 5.2 (0.3); | 1.0 (0.1); | 1500 |
| 20 | 7.7 (0.3); | 0.87 (0.08); | 1500 |
| 30 | 9.3 (0.4); | 0.74 (0.05); | 1500 |
| 100[b] | 900 (100); | 0.6 (0.1); | 20 |

[a] The experiments were carried out under a pressure of 6 bar at 298 K. Measurements performed with $\delta = 2$ ms. [b] Gas pressure was equal to 2.4 bar. The results were obtained in the original ZIF-8 powder with density 0.35 g $cm^{-3}$. [c] The SD in parentheses.

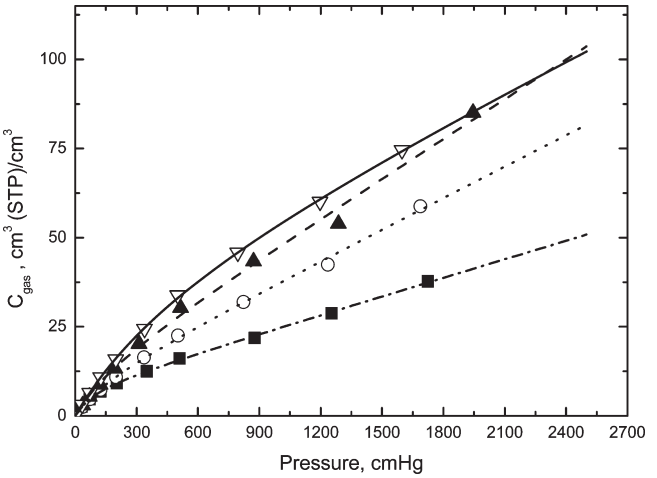


**Figure 8.** Variation of the concentration of carbon dioxide with pressure in (■) PPEES, (○) MMM-10, (▲) MMM-20, and (▽) MMM-30 membranes at 303 K.

unit for large values of the diffusion time (see Supporting Information). The fitting of eq 7 to the attenuation curves corresponding to the sorbed $[^{13}C]O_2$ in activated ZIF-8, prior to sonication, show that the diffusion coefficient for $\Delta = 20$ ms, under 2.4 bar of pressure, is $(9.0 \pm 1.0) \times 10^{-6}$ $cm^2\ s^{-1}$ with $\beta = 0.6 \pm 0.1$. Values of the apparent diffusion coefficient and stretching parameter, measured in membranes at 6 bar and at $\Delta = 1.5$ s, are collected in the second and third columns of Table 2, respectively.

Sorption curves showing the pressure dependence of the concentration of $CO_2$ in the membranes at 303 K are represented in Figure 8. As usual for sorption processes in glassy polymers, the curves exhibit a rather sharp increase with increasing pressure in the low-pressure region that become increasingly attenuated as pressure increases. The isotherms are described by the dual-mode model that assumes glassy membranes as made up of a continuous phase where the sorption process obeys Henry's behavior and another phase consisting of cavities or Langmuir sites that account for the excess volume where adsorption processes occur. The dependence of the concentration of gas on pressure in glassy polymers is given by[29,30,35,37]

$$c = k_D p + \frac{C'_H b p}{1 + b p} \tag{8}$$

where $k_D$ is Henry's constant, $C'_H$ is the concentration of gas in Langmuir sites, and $b$ is an affinity gas−polymer parameter. Strictly speaking, the values of $C'_H$ and $b$ in the polymer matrix will differ from those associated with the gas sorption in a variety of environments including matrix−ZIF-8 interfaces, polymer inside the filler pores, and pore fillers not containing polymer.

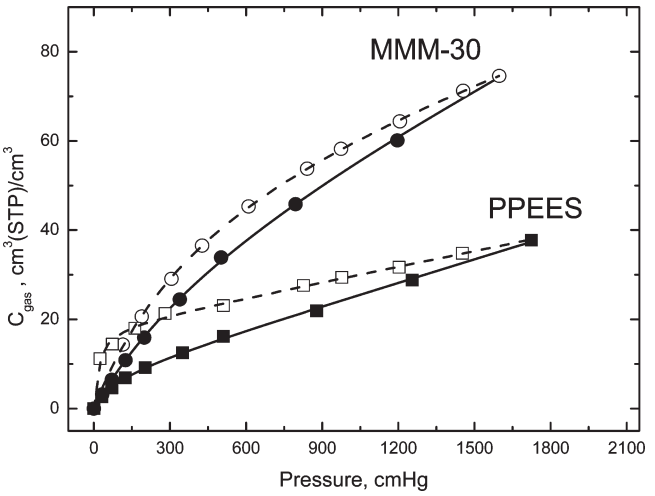


**Figure 9.** Variation of the concentration of sorbed (full symbols) and desorbed (open symbols) carbon dioxide with pressure for PPEES and MMM-30 at 303 K.

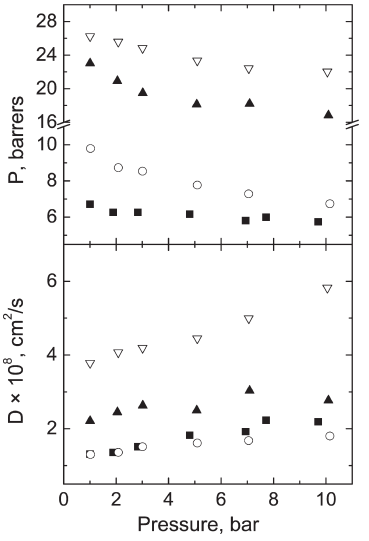


**Figure 10.** Variation of the permeability and diffusion coefficients of carbon dioxide with pressure, at 303 K, in membranes: (■) PPEES, (○) MMM-10, (▲) MMM-20, and (▽) MMM-30.

However, eq 8 fits rather well to the experimental results so that the values of $C'_H$, $b$, and $k_D$ represent the average of these sorption parameters in the variety of environments present in the MMMs. Values of the parameters of the dual-mode model that describe the $c$ vs $p$ curves for the PPEES membranes and the MMMs are shown in Table 1. Sorption results expressed in terms of the solubility coefficient (see Supporting Information) show that as expected for glassy polymers this coefficient decreases with increasing pressure, the limit values of this quantity being $k_D + bC'_H$ ($p \rightarrow 0$) and $k_D$ ($p \rightarrow \infty$). The values of the apparent solubility coefficient obtained from eq 3, also included in Supporting Information, are slightly lower than those directly obtained from sorption processes.

Illustrative gas desorption curves for PPEES and MMM-30 are shown in Figure 9. The sorption and desorption processes are not reversible, presenting a hysteresis cycle in which the sorption curves fall below the desorption ones. Moreover, eq 8 fits the desorption curves using the dual-mode model parameters given in Table 1.

Isotherms presenting the variation of the permeability coefficient of $CO_2$ with pressure in the PPEES membrane and the

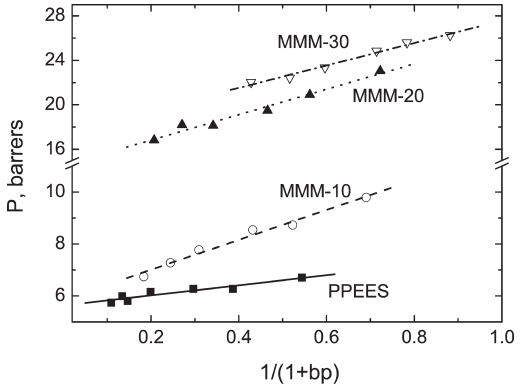


**Figure 11.** Fit of eq 9 to the experimental permeability coefficients of $CO_2$ in the membranes indicated in Figure 10.

**Table 3. Dual-Mode Model Parameters That Govern the Gas Permeation Characteristics of the Membranes at 303 K**

| sample | $k_D D_D$ (barrer) | $C'_H b D_H$ (barrer) | $D_D \times 10^8$ ($cm^2\ s^{-1}$) | $D_H \times 10^8$ ($cm^2\ s^{-1}$) | $D_H/D_D$ |
|---|---|---|---|---|---|
| PPEES | 5.63 | 1.95 | 3.27 | 0.21 | 0.06 |
| MMM-10 | 5.86 | 5.76 | 2.01 | 1.03 | 0.51 |
| MMM-20 | 14.54 | 11.43 | 3.96 | 1.74 | 0.44 |
| MMM-30 | 17.49 | 10.08 | 6.36 | 1.37 | 0.22 |

MMMs, at 303 K, are shown in Figure 10. As occurs with most gas permeation processes in glassy polymers, the values of $P$ decrease as $p$ increases, though the curvature of the isotherm diminishes with increasing $p$. Values of the diffusion coefficient of $CO_2$ in the membranes obtained from permeation experiments by means of eq 2 are also shown in Figure 10. The isotherms show that $D$ slightly increases with increasing pressure, an anomalous behavior presumably caused by $CO_2$ plasticization effects.

According to the partial immobilization dual-mode model, the evolution of the permeability coefficient with pressure is described by the following expression[35,37,38]

$$P = k_D D_D + \frac{C'_H b D_H}{1+bp} = k_D D_D \left[1 + \frac{FK}{1+bp}\right] \tag{9}$$

where $D_D$ and $D_H$ are respectively the diffusion coefficients in the continuous phase and Langmuir sites, $F = D_H/D_D$ is the mobile fraction of Langmuir species, and $K = bC'_H/k_D$. It is worth noting that eq 9 is a rather simplified approach because terms that couple the two modes are neglected.[39] By using for $b$ the results given in the fifth column of Table 1, the plots of $P$ against $1/(1+bp)$, shown in Figure 11, give reasonable straight lines from whose slopes and ordinates at the origin the values of $C'_H b D_H$ and $k_D D_D$, respectively, are obtained. Values of these parameters are shown in Table 3.

## Discussion

Since the skeletal and bulk densities of ZIF-8 are respectively 1.4 and 0.35 g $cm^{-3}$, the pores of the material occupy 75% of the volume.[40] Taking into account that the density of the unit crystalline cell of ZIF-8 (see Figure 1) is 0.93 g $cm^{-3}$, a substantial fraction of nonoccupied volume in ZIF-8 corresponds to pores resulting from the aggregation of crystals in the filler particles. In what follows, these pores will be called intercrystalline or interstitial pores. During the casting process polysulfone chains in the dilute solution may migrate into the pores of the filler. Thermodynamic arguments related with the variation of free energy taking place in the polymer coils as monomers of a single chain enter in nonadsorbing cylindrical pores of diameter $d_p$ indicate that the fraction of chain inside the cylinder is given by[41]

$$\psi \approx \exp\left[-\left(\frac{R_F}{d_p}\right)^{5/3}\right] \tag{10}$$

where $R_F = aN^{3.5}$ is the dimension of the chains, $N$ being the number of monomers of size $a$. Obviously, for $R_F \ll d_p$, isolated chains can penetrate into the pores. However, in absence of other driving forces, $\psi$ becomes negligible if $R_F \gg d_p$, though a solution of polymer coils may penetrate in the capillary[41−44] by effect of the osmotic pressure and other driving forces, such as flow, that tend to push the coils inside the empty capillary. The formation of depletion layers of correlation length $\xi(c)$, where $c$ is the concentration near the nonabsorbing walls may force the coils even in the cases $R_F \gg d_p$ inside the pores. Scaling laws for $\xi$ have been established that predict the critical concentration above which the pore is fully invaded by the polymer.

The effect of confined geometries on chains mobility may be reflected in the glass transition temperature. However, the MMMs exhibit a single $T_g$ similar to that of the polysulfone matrix, suggesting either that the pores of ZIF-8 are not partially occupied by the polymer chains or that the $T_g$ of the polymer inside the pores is not affected by its confinement. It should be indicated in this regard that experiments show a rich but nonuniversal behavior of the glass transition in confined geometries[45] in such a way that in some cases very large shifts of $T_g$ in thin films[46−48] and in pores[49,50] are observed. Thus, while the glass transition temperature is typically lower in confined geometries than in the bulk, there is also experimental evidence that in some cases $T_g$ undergoes an increase as well.[51−53] Therefore, from the analysis of the glass transition temperature of the MMMs no conclusions can be reached concerning the migration of polymer chains into the filler pores.

Assuming that the addition of volumes holds and the polysulfone chains penetrate neither into the filler intracrystal pores nor into the intercrystal ones, the density of the MMMs can be written as

$$\rho_{MMM} = \frac{\rho_{Z8}\rho_{PS}}{w_{Z8}\rho_{PS} + (1-w_{Z8})\rho_{Z8}} \tag{11}$$

where $w_{Z8}$ is the mass fraction of ZIF-8 in the MMMs whereas $\rho_{Z8}$ and $\rho_{PS}$ are respectively the bulk densities of ZIF-8 and PPEES. Taken as density of ZIF-8 in the MMMs that measured in bulk (0.35 g $cm^{-3}$), the densities of the membranes estimated by means of eq 11 are significantly lower than the experimental ones; for example, the density of MMM-30 would be only 0.70 g $cm^{-3}$, whereas the experimental one is 1.15 g $cm^{-3}$. To account for the values of the densities of the MMMs collected in the third column of Table 1 using the bulk density of ZIF-8, it is necessary to assume that the pores of the fillers are totally/partially occupied by PPEES chains.

Let us now consider the other extreme case, that the pores of the filler are totally filled by polymer chains. In this situation, the fraction of PPEES in the composite membranes, $w_{PS}$, not located in the pores of the MOFs, can roughly be estimated from the densities of the MMMs and the filler, using the following expression

$$w_{PS} = \frac{\rho_{PS}}{\rho_{MMM}} \frac{\rho_{Z8} - w_{Z8}\rho_{MMM}}{\rho_{Z8}} \tag{12}$$

In the development of this equation the volumes are assumed to be additive. The fraction of polymer outside the intra- and intercrystal pores of ZIF-8 is 0.671, 0.379, and 0.015 respectively

for MMM-10, MMM-20, and MMM-30. According to this assumption, nearly all the PPEES coils would occupy the intra- and intercrystal pores of ZIF-8 in the MMM-30 composite membrane. However, an inspection of the cross section of the MMM-30 obtained by SEM technique shows zones in the membranes where filler particles are absent. Moreover, an inspection of the SEMs of the composite membranes shows that the size of the particles dispersed in the polysulfone matrix may be nearly one-tenth of that corresponding to the particles of the original ZIF-8 powder. Then, the sonication process involved in the preparation of membranes reduces the particles size, and as a result, the intercrystal pore volume arisen from the aggregation of different crystal entities decreases. In this case, the density of the filler dispersed in the polymer matrix must be significantly higher than that of the original ZIF-8. In the absence of intercrystal pores, the density of ZIF-8 is 0.93 g $cm^{-3}$. Assuming this latter density for the ZIF-8 dispersed in the MMMs, the densities estimated for MMM-10, MMM-20, and MMM-30 are respectively 1.20, 1.16, and 1.13 g $cm^{-3}$, in rather good agreement with the experimental values measured by pycnometry, collected in the third column of Table 1. Accordingly, intercrystal pores are mostly destroyed in the sonication process, and the diffusion coefficient of $CO_2$ in the ZIF-8 particles dispersed in the MMMs should be substantially lower than that measured in the non-sonicated filler, with density 0.35 g $cm^{-3}$.

In the pristine polysulfone membrane, the carbon-13 transverse relaxation time, $T_2$, of $[^{13}C]O_2$ is very short, and the echo signal decays very rapidly with increasing echo times. In this case, a pulse field gradient stimulated spin-echo pulse sequence was used taking advantage of the longitudinal relaxation time, $T_1$, for the gas in the polysulfone membrane which is ca. 3 s for this system, and the sequence allows relatively short echo times (2−4 ms). Using a diffusion time of 20 ms and pulse gradients of 2 ms, the value obtained for the apparent diffusion coefficient of $[^{13}C]O_2$ in the PPEES membrane was $(2.1 \pm 0.9) \times 10^{-8}$ $cm^2$ $s^{-1}$. The accuracy of the value of $D$ obtained at $\Delta = 20$ ms is made evident by the fact that it is similar to that determined for the polysulfone membrane from permeation measurements carried out at the same pressure. Moreover, diffusion times larger than 10 ms properly averages the diffusive paths associated with different environments in pristine glassy membranes.[54,55] Additional information is provided in the Supporting Information.

Diffusive paths in MMMs take place in a wide variety of environments involving the polymer matrix, matrix−ZIF-8 interfaces, and pores of the filler. To accomplish a good average of diffusive trajectories in this variety of environments requires more time than in pristine membranes. This fact is reflected in Figure 7 where a screening on the influence of the diffusion time on the diffusion coefficient of $[^{13}C]O_2$ in the MMMs is shown. It can be seen that a constant value of $D_{app}$ is obtained for diffusion times larger than 800 ms. Owing to the fact that the square root of the mean-square displacement of the probe is $\langle r^2 \rangle^{1/2} = (6D\Delta)^{1/2}$, constant values of $D$ are the result of averaging trajectories at mesoscopic scale. Actually, at diffusion times of 800 ms, the values of $\langle r^2 \rangle$ in $\mu$m units are 5.0, 6.0, and 6.8 for MMM-10, MMM-20, and MMM-30, respectively. On the other hand, the results obtained for the stretching parameter that fits eq 7 to the PFG NMR attenuation curves show that the values of $\beta$ increase as the diffusion time increases. This behavior suggests that at short times the environmental places where diffusion occurs is rather heterogeneous a fact reflected in the relatively low value of $\beta$. The environmental heterogeneity progressively decreases as the time of exposure increases, eventually $\beta$ reaching a value close to the unit at relatively large values of $\Delta$ (see Figure 5 of the Supporting Information). Accordingly, the true weight of slow diffusion processes that control the diffusive step can only be observed at rather long times in the case of MMMs.

According to the partial immobilized dual-mode model, Langmuir mode species can partly be immobilized in glassy MMMs. The analysis of the permeation results at the light of the partial immobilized mode yields for $C'_H b D_H$ and $k_D D_D$ the results given in Table 3. By combining these results with the values of $C'_H$ and $k_D$ obtained from the pertinent sorption experiments given in Table 1, the individualized values of the apparent diffusion coefficient of $CO_2$ in the continuous phase of the membrane, $D_D$, and the Langmuir sites, $D_H$, are estimated. For the polysulfone membrane $D_H = 0.06 D_D$, but the value of this parameter undergoes a substantial increase with the presence of ZIF-8 particles in the MMMs in such a way that $D_H = 0.51 D_D$ for the MMM-10.

The concentration of gas in the membrane is $C = C_D + C_H$ where, according to eq 8, $C_H = C'_H bp/(1 + bp)$ and $C_D = k_D p$. Assuming that the partial immobilized model holds, the flux of gas across the membranes in steady state conditions can be written as

$$J = -D_D \left[ \frac{1 + \frac{FK}{(1+bp)^2}}{1 + \frac{K}{(1+bp)^2}} \right] \frac{\partial C}{\partial x} = -D_{DM}(C) \frac{\partial C}{\partial x} \qquad (13)$$

where

$$D_{DM}(C) = D_D \left[ \frac{1 + \frac{FK}{(1+bp)^2}}{1 + \frac{K}{(1+bp)^2}} \right] \qquad (14)$$

The reliability of the dual-mode model parameters used to calculate $D_{DM}$ from eq 14 can be estimated from the flux of the gas across a membrane in steady-state conditions. The pertinent equations for $J$ in terms of pressure and concentration are

$$J = D_{eff}(C) C/l = P(p) p/l \qquad (15)$$

where $D_{eff}$ is an effective diffusion coefficient that depends on concentration and $l$ is the membrane thickness whereas $C$ and $p$ are respectively the concentration and pressure of the gas in the upstream chamber. From the pressure dependence of the flux $J$, $dJ/dp$, eq 15 leads to

$$D_{eff}(C_i) = \left[ P(p) + p \frac{\partial P(p)}{\partial p} \right]_{p_i} \left( \frac{\partial p}{\partial C} \right)_{p_i} \qquad (16)$$

where $C_i$ is the concentration of gas in the membrane at pressure $p_i$ in the $p$ vs $C$ sorption curves. This expression was earlier used by Koros et al.[35] to check the reliability of the partial immobilization model. Values of the diffusion coefficient obtained from eqs 14 and 16 and the time lag method for PPEES and MMM-20 membranes are shown as a function of concentration in Figure 12. It can be seen that in the whole pressure range $D_{eff} \cong D_{DM}$ for PPEES and MMMs, whereas the diffusion coefficient obtained by the time lag, $D_\theta$, is lower than $D_{eff}$ for PPEES, MMM-10, and MMM-20. Also, the values of the diverse diffusion coefficients increase as the filler content increases, except in the case of the MMM-10 where the values of $D_{eff}$, $D_{DM}$, and $D_\theta$ are slightly smaller than the respective values of these coefficients corresponding to PPEES. For illustrative purposes, the results for $D_{eff}$, $D_{DM}$, and $D_\theta$ obtained at 6 bar are compared with those measured by PFG NMR, at the same pressure, in Table 4. The discrepancies observed between the values of $D_\theta$ and those of $D_{eff}$ and $D_{DM}$ may arise from shortcomings associated with the method used to evaluate $D_\theta$. Actually, the time lag method is based on the assumption that the diffusion coefficient is independent of concentration in the integration of Fick's second law,

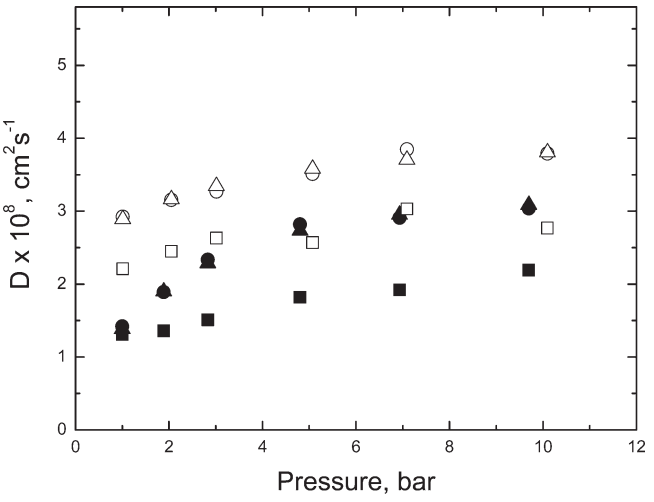


**Figure 12.** Variation of the diffusion coefficients of $CO_2$ obtained from the time lag method eq 2, $D_\theta$ (squares), the dual-mode model eq 14, $D_{DM}$ (up-triangles), and permeation-sorption results eq 16, $D_{eff}$ (circles), with pressure in PPEES (closed symbols) and MMM-20 (open symbols) membranes.

**Table 4. Summary of Values of $CO_2$ Diffusion Coefficients Expressed in $cm^2\ s^{-1}$, at 303 K and 6 bar, in PPEES and MMMs, as Well as in ZIF-8, Determined by the Dual-Mode Model (Eq 14), $D_{DM}$, Permeation and Sorption Results (Eq 16), $D_{eff}$, the PFG NMR Technique (Eq 7), $D_{NMR}$ ($D_{app}$), and the Time Lag Method $D_\theta$ (Eq 2)**

| sample | $D_{NMR}$[a] $\times 10^8$ | $D_\theta \times 10^8$ | $D_{eff} \times 10^8$ | $D_{DM} \times 10^8$ |
|---|---|---|---|---|
| PPEES | 2.1 | 1.87 | 2.87 | 2.84 |
| MMM-10 | 5.2 | 1.65 | 1.91 | 1.89 |
| MMM-20 | 7.7 | 2.80 | 3.68 | 3.65 |
| MMM-30 | 9.3 | 4.72 | 4.09 | 4.14 |
| ZIF-8 | 900[b] | | | |

[a] Measurements performed at 298 K. [b] Experiments were carried out in ZIF-8 as received ($\rho = 0.35$ g cm$^{-3}$) under gas pressure of 2.4 bar.

and this is not the case in our systems. The determination of $D_{DM}$ requires to know with precision good enough the dual-mode model parameters associated with the sorption and diffusive steps since small variations in them strongly affect the values of $D_M$. $D_{eff}$ can directly be calculated from permeability and concentration data, and from this point of view, the values obtained for this parameter should be more reliable than the alternative results obtained for $D_\theta$ and $D_{DM}$. The good agreement between the values of $D_{eff}$ and $D_{DM}$ validates the reliability of the dual-mode model parameters obtained by fitting eqs 8 and 9 to the sorption and permeation results.

In the PFG NMR technique, the concentration of gas is homogeneous across the samples so that the self-diffusion coefficient of $CO_2$ in the membranes is obtained. The self-diffusion coefficient of $CO_2$ in pristine membranes is rather similar to the apparent diffusion coefficients obtained by sorption and permeation techniques. However, the self-diffusion coefficient of $CO_2$ in the MMMs is roughly 2 times $D_{eff}$ or $D_M$. For diffusion times near to 800 ms, the self-diffusion coefficient is obtained from trajectories whose square root of the mean end-to-end distance $\langle r^2\rangle^{1/2}$ lies in the range between 5.0 and 6.8 $\mu$m for the MMMs. In this case, it is hard to imagine rapid trajectories accounted for in the technique that enhance the self-diffusion coefficient of $CO_2$. Moreover, the self-diffusion coefficients remain constant if the respective values of $\langle r^2\rangle^{1/2}$ for the MMMs increase 141%. The insensitivity of the self-diffusion coefficients to $\langle r^2\rangle$ for $\Delta > 800$ $\mu$s supports the reliability of the self-diffusion coefficients obtained by PFG NMR. Then the values of $D(c)$ obtained by sorption and permeation experiments may be somewhat underestimated.

In general, the solubility coefficient of the gases increases as the ZIF-8 content in the membrane increases. As shown in the Supporting Information, the absolute values of the solubility coefficient at 1 bar are in most cases somewhat higher than the apparent solubility coefficients obtained from the $P/D$ ratio. The increase in the absolute values of $S$ is a consequence of the fact that the concentration of $CO_2$ in Langmuir sites increases as the filler content increases. Henry's solubility constant seems to be slightly higher in the MMMs than in the PPEES membrane, though the value of this quantity in the composite membranes does not follow a definite trend. Owing to the nonequilibrium state of glassy polymers, gas sorption and desorption in both the polysulfone membrane and the MMMs exhibit hysteresis cycles,[56,57] a manifestation of the long relaxation times associated with the glassy state. Notice that for rubbery polymers where relaxation times are very short, sorption and desorption curves coincide.[57] An inspection of the sorption and desorption curves presented for PPEES and MMM-30 in Figure 9 shows that the hysteresis behavior is larger for the former system than for the latter in accordance with the glassy polymer content. Accordingly, the hysteresis associated with the sorption−desorption process follows the trend PPEES > MMM-10 > MMM-20 > MMM-30.

## Conclusions

In summary, mixed matrix membranes of PPEES with ZIF-8 were prepared and characterized, and the transport properties were investigated by macroscopic and microscopic techniques. The SEM results show that the size of the ZIF-8 particles is reduced after sonication, but the crystal structure does not change as confirmed by X-ray analysis. The sonication process destroys most intercrystal pores in such a way that the densities of the MMMs estimated from the densities of PPEES and ZIF-8 crystals are similar to those measured by pycnometry. Accordingly, the fraction of polymer in the intercrystal pores is negligible.

PFG NMR results show that diffusion times on the order of 1000−1500 ms are necessary to reach a constant value of the diffusion coefficient of $CO_2$ in the MMMs, highlighting the fact that the technique needs a rather high time to average appropriately the diffusive environments encountered in the composite membranes. The cause of this behavior lies in the heterogeneity of environments that polymer matrix, polymer−filler interface, and partial occupation of the pores of ZIF-8 by the polysulfone chains provide. The self-diffusion coefficient of $CO_2$ in pristine PPEES membranes is similar to the apparent diffusion coefficients obtained by permeation and sorption techniques. However, for composite membranes, the self-diffusion coefficient is nearly 2 times that of $D_{eff}$. The fact that averages carried out on trajectories obtained at progressively increasing diffusion time yield nearly constant values for the self-diffusion coefficient validate the results obtained for this parameter using the PFG NMR technique.

ZIF-8 crystals provide Langmuir sites where adsorption of $CO_2$ molecules may take place, and as a result, the gas adsorption in the MMMs increases as the filler content increases.

**Acknowledgment.** The authors acknowledge the financial support provided by DGPA-UNAM (Project IN112109), IMPULSA (Proyecto PUNTA), Comunidad de Madrid (CAM S-0505/MAT/0227), and CICYT (MAT2005-05648-C02-01). Also, K.D. acknowledges CONACyT for a PhD scholarship. We are enormously grateful to Leticia Baños, Miguel Canseco, Gerardo Cedillo, and Esteban Fregoso for their technical assistance with powder X-ray, IR, and TGA (thermal properties) and to David Gómez of ICTP with SEM micrographs.

**Supporting Information Available:** Experimental details. This material is available free of charge via the Internet at http://pubs.acs.org.

## References and Notes


(1) Robeson, L. M. *J. Membr. Sci.* **1991**, *62*, 165. *J. Membr. Sci.* **2008**, *320*, 390.Robeson, L. M.; Freeman, B. D.; Paul, D. R.; Roweb, B. W. *J. Membr. Sci.* **2009**, *341*, 178 (Robeson has established an empirical upper bound relationship for membranes separation of gases using myriad of data available in the literature. Below the line of log $\alpha_{ij}$ ($= P_i/P_j$) vs log $P_i$, where $P_i$ is the permeability of the fast gas, virtually all the experimental data points exist) .
(2) Freeman, B. D. *Macromolecules* **1999**, *32*, 375.
(3) Mahajan, R.; Koros, W. J. *Ind. Eng. Chem. Res.* **2000**, *39*, 2692.
(4) Mahajan, R.; Koros, W. J. *Polym. Eng. Sci.* **2002**, *42*, 1420. *Polym. Eng. Sci.* **2002**, *42*, 1432.
(5) Kim, S.; Marand, E.; Ida, J.; Guliants, V. V. *Chem. Mater.* **2006**, *18*, 1149.
(6) Pechar, T. W.; Kim, S.; Vaughan, B.; Marand, E. M.; Baranauskas, V.; Riffles, J.; Jeong, H. K.; Tsapatsis, M. *J. Membr. Sci.* **2006**, *277*, 210.
(7) Reid, B. D.; Ruiz Treviño, F. A.; Musselman, I. H.; Balkus, K. J.; Ferraris, J. P. *Chem. Mater.* **2001**, *13*, 2366.
(8) Shu, S.; Husain, S.; Koros, W. *AIChE J.* **2004**, *50*, 311.
(9) Zhang, Y.; Li, H.; Lin, J.; Li, R.; Liang, X. *Desalination* **2006**, *192*, 198.
(10) Shu, S.; Husain, S.; Koros, W. J. *J. Phys. Chem. C* **2007**, *111*, 652.
(11) Chung, T.; Chan, S.; Wang, R.; Lu, Z.; He, C. *J. Membr. Sci.* **2003**, *211*, 91.
(12) Kim, S.; Pechar, T. W.; Maranda, E. *Desalination* **2006**, *192*, 330.
(13) Sun, D.; Collins, D. J.; Ke, Y.; Zuo, J.-L.; Zhou, H.-C. *Chem.—Eur. J.* **2006**, *12*, 3768.
(14) Sun, D.; Ma, S.; Ke, Y.; Petersen, T. M.; Zhou, H.-C. *Chem. Commun.* **2005**, 2663.
(15) Snurr, R. Q.; Hupp, J. T.; Nguyen, S. T. *AIChE J.* **2004**, *50*, 1090.
(16) Eddaoudi, M.; Kim, J.; Rosi, N.; Vodak, D.; Wachter, J.; O'Keefe, M.; Yaghi, O. M. *Science* **2002**, *295*, 469.
(17) Düren, T.; Sorkisov, L.; Yaghi, O. M.; Snurr, R. Q. *Langmuir* **2004**, *20*, 2683.
(18) Ma, S.; Sun, D.; Simmons, J. M.; Yuan, D.; Zhou, H.-C. *J. Am. Chem. Soc.* **2008**, *130*, 1012.
(19) Zhao, X. B.; Xiao, B.; Fletcher, A. J.; Thomas, K. M.; Bradshaw, D.; Rosseinsky, M. J. *Science* **2004**, *306*, 1012.
(20) Chen, B. L.; Ockwig, N. W.; Millward, A. R.; Contreras, D. S.; Yaghi, O. M. *Angew. Chem., Int. Ed.* **2005**, *44*, 4745.
(21) Zhao, D.; Yuan, D.; Zhou, H.-C. *Energy Environ. Sci.* **2008**, *1*, 122.
(22) Millward, A. R.; Yaghi, O. M. *J. Am. Chem. Soc.* **2005**, *127*, 17998.
(23) Zhan, Y.; Musselman, I. H.; Ferraris, J. P.; Balkus, K. J., Jr. *J. Membr. Sci.* **2008**, *313*, 170.
(24) Park, K. S.; Ni, Z.; Côté, A. P.; Choi, J. Y.; Huang, R.; Uribe-Romo, F. J.; Chae, H. K.; O'Keeffe, M.; Yaghi, O. M. *PANS* **2006**, *103*, 10186. Banerjee, R.; Furukawa, H.; Britt, D.; Knobler, C.; O'Keeffe, M.; Yaghi, O. M. *J. Am. Chem. Soc.* **2009**, *131*, 3875.
(25) Huang, C.; Ci, X.; Lin, Y. Y.; Zhang, J. P.; Chen, X. M. *Angew. Chem., Int. Ed.* **2006**, *45*, 1557.
(26) Wang, B.; Côté, A. P.; Furukawa, H.; O'Keeffe, M.; Yaghi, O. M. *Nature* **2008**, *453*, 207.
(27) Kärger, J.; Pfeifer, H.; Heink, W. *Adv. Magn. Reson.* **1988**, *12*, 2. Price, W. S. *Concepts Magn. Reson.* **1997**, *9*, 299.
(28) Callaghan, P. T. In *Principles of Nuclear Magnetic Resonance Microscopy*; Oxford University Press: New York, 1991; Chapter 6.
(29) Vieth, W. R.; Howell, J. M.; Hsieh, J. H. *J. Membr. Sci.* **1976**, *1*, 177.
(30) Paul, D. R. *Ber. Bunsen-Ges.* **1979**, *83*, 294.
(31) Louer, D.; Vargas, R. *J. Appl. Crystallogr.* **1982**, *15*, 542.
(32) Stejskal, E. O.; Tanner, J. E. *J. Chem. Phys.* **1965**, *42*, 288.
(33) Callaghan, P. T.; Jolley, K. W.; Trotter, C. M. *J. Magn. Reson.* **1980**, *39*, 525.
(34) Barrer, R. M. *Trans. Faraday Soc.* **1939**, *35*, 628.
(35) Koros, W. J.; Paul, D. R.; Rocha, A. A. *J. Polym. Sci., Polym. Phys. Ed.* **1976**, *14*, 687.
(36) Wen, W. Y. *Chem. Soc. Rev.* **1993**, *22*, 117.
(37) Paul, D. R.; Koros, W. J. *J. Polym. Sci., Polym. Phys. Ed.* **1976**, *14*, 675.
(38) Kesting, R. E.; Fritzsche, A. K. In *Polymeric Gas Separation Membranes*; Wiley-Interscience: New York, 1993; p 32.
(39) Frederickson, G. H.; Helfand, E. *Macromolecules* **1985**, *18*, 2201.
(40) Wei, Z.; Hui, W.; Hartman, M. R.; Yildirim, T. *J. Phys. Chem. C* **2007**, *111*, 16131.
(41) de Gennes, P. G. In *Transport of Polymers In Disorder and Mixing*; Guyon, E., Nadal, J. P., Pomeau, Y., Eds.; NATO ASI Series E; Kluwer Academic Publishers: Dordrecht, 1988; Vol *152*, Chapter 12.
(42) Guillot, G.; Léger, L.; Rondelez, F. *Macromolecules* **1985**, *18*, 2531.
(43) Bagassi, M. Comportement hydrodynamique des macromolécules dans les milieux poreux fins en régime d deformation faible. Thèse Université de Bretagne Occidentale, Brest, **1986**.
(44) de Gennes, P. G. In *Scaling Concepts in Polymer Physics*, 2nd ed.; Cornell University Press: Ithaca, NY, 1985; Chapter 6.
(45) McCoy, J. D.; Curro, J. G. *J. Chem. Phys.* **2002**, *116*, 9154.
(46) Forrest, J. A.; Dalnoki-Veress, K.; Stevens, J. R.; Dutcher, J. R. *Phys. Rev. Lett.* **1996**, *77*, 2002.
(47) Forrest, J. A.; Mattsson, J. *Phys. Rev. E* **2000**, *61*, R53.
(48) Dalnoki-Veress, K.; Forrest, J. A.; Murray, C.; Gigault, C.; Dutcher, J. R. *Phys. Rev. E* **2001**, *63*, 031801.
(49) Jackson, C. L.; McKenna, G. B. *Chem. Mater.* **1996**, *8*, 2128.
(50) Park, J.-Y.; McKenna, G. B. *Phys. Rev. B* **2000**, *61*, 6667.
(51) Fryer, D. S.; Nealey, P. F.; dePablo, J. J. *Macromolecules* **2000**, *33*, 6439.
(52) Schuller, J.; Melnichenko, Y. B.; Richert, R.; Fisher, E. W. *Phys. Rev. Lett.* **1994**, *73*, 2224.
(53) Schuller, J.; Richert, R.; Fisher, E. W. *Phys. Rev. B* **1995**, *52*, 15232.
(54) Garrido, L.; López-González, M.; Saiz, E.; Riande, E. *J. Phys. Chem.* **2008**, *112*, 4253.
(55) Garrido, L.; López-González, M.; Riande, E. *J. Polym. Sci., Part B: Polym. Phys.*, in press.
(56) Fleming, G. K.; Koros, W. J. *Macromolecules* **1986**, *19*, 2285.
(57) Fleming, G. K. Ph.D. Dissertation, The University of Texas at Austin, **1987**.